Space Robotic De-Tumbling of Large Target with Eddy Current Brake in Hand

Jiayu Liu[1,2(✉)], Baosen Du[2], and Qiang Huang[1]

[1] School of Mechatronical Engineering, Intelligent Robotics Institute, Beijing Institute of Technology, 5 Nandajie, Zhongguancun, Haidian, Beijing, China
jyliu_bit@hotmail.com
[2] Beijing Institute of Precise Mechatronics and Controls (the 18th Institute), China Academy of Launch Vehicle Technology (CALT), 1 Nandahongmenlu, Fengtai, Beijing, China

Abstract. Space debris has increased with recent launch missions greatly. Former active debris removal tests using space robot mainly focused on the fundamental technology of target recognition, motion control and path planning. However, robot contacts directly with the surface of targets with large mass and angular momentum will cause severe collision problems. A target de-tumbling strategy is proposed in this paper by using two manipulators. Each arm is equipped with magnetic coil, which can generate eddy current in conductive targets and gradually de-tumble rotation without contact. The three-dimension rotation model of a discarded satellite and upstage is established based on its distribution of the moment of inertia and the safe working space of the robots is calculated. By analyzing the point of application and direction of the magnetic force, an optimized de-tumbling trajectory for the robot is presented to minimize the de-tumbling time by reducing the targets' angular momentum. At last, a simulation is processed to verify the optimized de-tumbling method.

Keywords: Space robot · Eddy current brake · On-orbit · Tumbling target · Large debris capture

1 Introduction

Satellites in orbit have greatly increased in recent years with the unceasing space development. With the limited space resources, space debris removal should be taken into action to make better use of the space.

1.1 Typical Target Capture Method

The debris removal method includes active debris removal and passive debris removal method. Passive debris removal usually puts a damper on the debris and drag it to the atmospheric layer by earth magnetic field or pneumatic forces. Active debris removal needs a space craft to perform the capture of the debris and then remove it with the spacecraft's energy. And this removal procedure often equips with manipulator.

Y. Huang et al. (Eds.): ICIRA 2017, Part III, LNAI 10464, pp. 637–649, 2017.
DOI: 10.1007/978-3-319-65298-6_57

1.2 Target Manipulation with Manipulator

Robot manipulator, also named robotic arm, has been used in on-orbit refueling, module replacement and assisted space docking. These robot arms have different D-H parameters and joint numbers [1–3]. And researches on robot arms have extended to multi-robot and dedicated operation from single robot. Some research work focused on the eddy current brake have got wonderful results [4–7].

Chaser with a manipulator de-tumbles a large tumbling debris with an eddy current brake is shown in Fig. 1, and this paper is focused on the challenge.

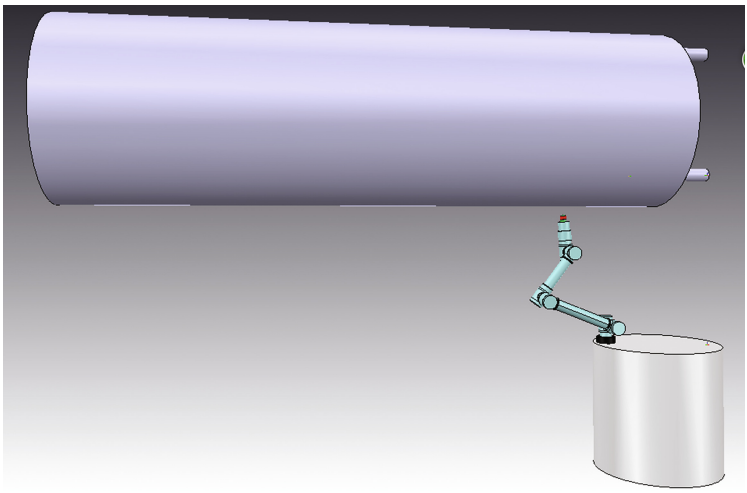

Fig. 1. De-tumbling of large target with Eddy Current Brake in Hand

1.3 Problems of Debris with High Angular Momentum

Former debris target to be captured by robot arm often has such characters: a, the target's attitude is limited, it has a relatively constant pose to the spacecraft. b, the target is small and little in weight, it is easy to be handled by the robot arm's gripper. c, the target's angular velocity is negligible, the spacecraft can keep still to the target by orbital maneuver.

However, debris generated in recent years are mainly satellites and abandoned rocket's upper stage which are large and weight. And these debris also have angular velocity which lead to large angular momentum.

Traditional method using rigid gripper to directly contact with the debris has following problems: a, the gripper may break at this moment when the arm first contact with the debris. b, the enormous torque transferred from the debris after the manipulator has linked to the debris may cause the joint motor to break down or even break the transmission gear. c, the sudden impact may cause the spacecraft out of control. d, the impact may drive the debris away and out of sight.

In this paper, a contactless debris removal strategy is proposed to accomplish the de-tumbling procedure of debris with large angular momentum. And avoid the problem of rigid contact by using eddy current brake. The kinematic model of the debris in spin state is established to analyze the de-tumbling procedure. Then an optimized de-tumbling method is proposed by calculation referring time consuming. At last, a simulation is designed to illustrate the efficiency of optimized strategy.

2 Target Recognition and De-Tumbling

The capture system consists of two parts: the target to be captured, meaning the space debris in orbit with large mass; the performer of the capture mission, meaning the space craft with manipulator on board.

The chaser keeps the target in the robot arm's manipulation space by attitude adjustment after it reaches the target's zone by orbital maneuver.

The eddy current brake in the hand of the manipulator starts to work after the manipulator has moved to the target coordinate by path planning. It will then gradually decrease the target's spin movement. At the same time, the controller system maintains the chaser-target's relative position and the manipulator's action pose by real-time calculation.

2.1 Target Approach and Coordinates Building

The target's orbit is assessed by observation, then the chaser can fly to the target's zone through orbital maneuver Fig. 2.

Typical capturing method as described here is called active debris removal strategy. Debris in the orbit is the target of the chaser-target system while the capture vehicle acting as the chaser. First, the orbit of the target debris is observed.

When the chaser reaches the same orbit with the target. It slowly changes its relative pose to the target while maintaining their position until the end effector of the onboard manipulator is in flexible manipulation space.

The spinning motion of the target rotating around the coordinate axes can be reconstructed by vision camera. Two different frames are built here to explain the

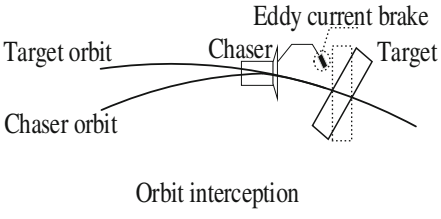

Fig. 2. Capturing of large tumbling target

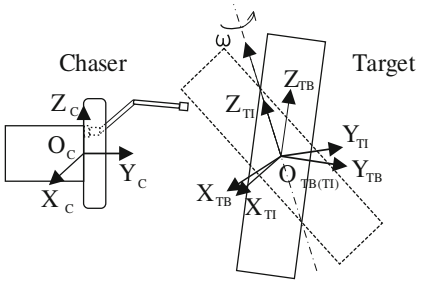

Fig. 3. Coordinates of target and chaser

target's angular velocity and angular momentum. The body frame's origin of coordinate is the center of mass of the debris. And set the minimum inertia spindle as the Z_{TB} axis. And X_{TB}, Y_{TB} axes are mutually perpendicular in the transection of the cylinder. Then the complex spin kinematic of the target can be described as rotation movement around three perpendicular axes OX_{TB} OY_{TB} OZ_{TB} with the angular velocity ω_X ω_Y ω_Z.

The origin of the inertia frame is also the target's center of mass. Set ω as the resultant vector of angular velocity's component ω_X ω_Y ω_Z. Then the inertia frame's Z_{IB} axis is parallel to ω.

In the same way, the chaser's body frame can be built based on the center of its load's setting surface. Y_C axis is perpendicular to the manipulator's fixing panel Fig. 3.

First, when the captor reaches the target's spin zone, maintaining the relative position between the spacecraft and the target.

$$P_{O_C}^{O_{TI}} = const \tag{1}$$

Then, keeping the three axes of the captor's body frame parallel to that of the target's inertia frame by adjusting the spacecraft's spatial attitude.

$$R_{O_CXYZ}^{O_{TI}XYZ} = \begin{bmatrix} 1 & 0 & 0 \\ 0 & 1 & 0 \\ 0 & 0 & 1 \end{bmatrix} \tag{2}$$

$$T_{O_CXYZ}^{O_{TI}XYZ} = \begin{bmatrix} R_{O_CXYZ}^{O_{TI}XYZ} & P_{O_C}^{O_{TI}} \\ 0 & 1 \end{bmatrix} = const \tag{3}$$

By this way, the position and orientation matrix between the target's inertia frame and the captor's body frame is established. The manipulator onboard can calculate the target's position through coordinate translation.

From [8–11], the dynamics motion of target with external force from action point between hand and target can be described as:

$$H_t\ddot{r}_t + C_t = J_t^T f_{hd} \tag{4}$$

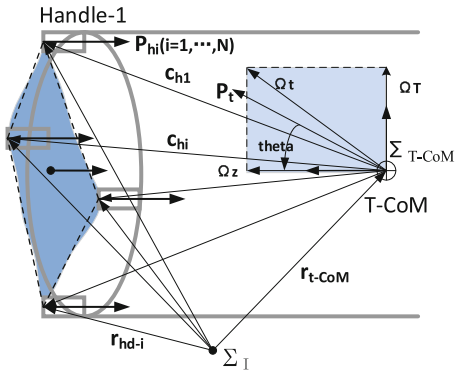

Fig. 4. The model of rocket upstage

Where, $\ddot{r}_t = \mathrm{col}(p_t, \varphi_t) \in \Re^6$ is the generalized velocity vector consisting of the position of the center of mass $p_t \in \Re^3$ and the attitude $\varphi_t \in \Re^3$, respectively. Figure 4$C_t \in \Re^6$ represents the centrifugal and Coriolis terms. The vector $f_{hd} \in \Re^6$ is the force and moment exerted by the arms. $H_t \in \Re^{6\times6}$ is the generalized mass matrix which can be described as:

$$H_t = \begin{bmatrix} m1 & 0 \\ 0 & I_c \end{bmatrix} \tag{5}$$

Where, m and I_c denote the mass and the inertia tensor of the target, respectively.

$$c_t = \begin{bmatrix} m\tilde{\omega}_t v_0 \\ \tilde{\omega}_t I_c \omega_0 \end{bmatrix} \tag{6}$$

Generalized Jacobin matrix A^k can be described following with $\rho \in \Re^3$ being the position vector of the k^{th} action point with respect to its center of mass which detailed in 8. The operator $\sim$ hat a vector denotes the cross product with the following vector.

$$J_t^k = \begin{bmatrix} 1_3 & \widetilde{\rho}_k \\ 0 & 1_3 \end{bmatrix} \tag{7}$$

At this point, the dynamic model of the tumbling target has been established, and the follow-up will carry out the study of the trajectory optimization of de-tumbling planning with eddy current brake based on the motion characteristics of the tumbling target.

2.2 Contactless De-Tumbling

The relative pose between the target and the manipulator's end effector can be determined when the pose between the end and the robot's base frame, the pose between the robot's base frame and the captor's body frame, the pose between the target's inertia frame and the captor's body frame. And the target's pose in its inertia frame are determined.

A constant magnetic field will be generated when the eddy current brake at the robot's end is powered on. During the de-tumbling procedure, make sure the brake is close to the external surface of the target's spin state with the magnetic field's direction parallel to the external surface's normal direction. Current is produced when the target moves cutting the magnetic induction lines. And the direction of the force F_B produced by the brake is opposed to the target's movement Fig. 5.

By keeping the magnetic induction lines' direction perpendicular to the direction of the target's resultant vector ω and the brake close to the target, an electromagnetic torque will continually decrease the target's angular momentum. And eventually makes the target captured by the captor.

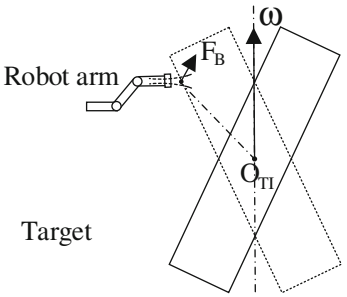

Fig. 5. Brake force by eddy current

3 Optimization of De-Tumbling Strategy

As the brake force's direction is always opposed to the target's movement and the action time is relative to the brake's shape size and the relative speed between the target and the manipulator. The major factor that affects the de-tumbling torque's performance is the brake force's point of action. In this section, the de-tumbling procedure of the target by cutting down its angular momentum through eddy current brake is analyzed. And an optimized de-tumbling strategy is proposed referring to time consuming.

3.1 Dynamics of Target De-Tumbling

The relationship between the target's angular velocity vector and angular momentum is shown as below when it is in spin state Fig. 6.

The target's Euler equations of spin movement in orbit are:

$$\begin{aligned} J_x\dot{\omega}_x + \omega_x \times J_x\omega_x &= \sum T_x \\ J_y\dot{\omega}_y + \omega_y \times J_y\omega_y &= \sum T_y \\ J_z\dot{\omega}_z + \omega_z \times J_z\omega_z &= \sum T_z \end{aligned} \tag{8}$$

The angular velocity around X Y Z axes remain unchanged when the target's resultant momentum is zero, and can be expressed as below:

$$\begin{aligned} H_x &= J_x\omega_x \\ H_y &= J_y\omega_y \\ H_z &= J_z\omega_z \end{aligned} \tag{9}$$

Usually, the target's angular velocity vector is not parallel to its angular momentum vector. The eddy current brake generates the angular momentum H_F by applying the brake force F_B on the target to decrease the target's angular momentum H Fig. 7.

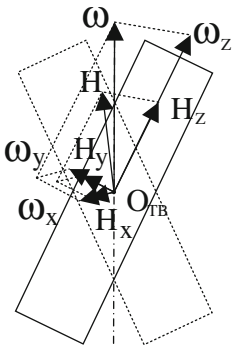

Fig. 6. Rotation model

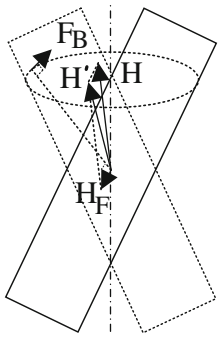

Fig. 7. Angular momentum of target

The eddy-current-brake angular momentum applies once when the target circles one time around its angular velocity vector. And the target's angular momentum is decreased from H to H′. Which also means a decrease in the target's angular velocity. Its angular velocity turns out to be zero by continuous de-tumbling method.

3.2 Calculation of Optimized De-Tumbling Strategy

The eddy-current-brake angular momentum vector's value and direction depends on the brake force's point of action.

The total time to finish the de-tumbling procedure is set as the principle to judge the strategy's efficiency. The less the remained angular momentum of the target is after one revolution, the better the de-tumbling strategy is.

So, the optimized de-tumbling strategy is to find out the minimum value of H'.

$$\mathrm{Min}\{H'\} \tag{10}$$

Assuming the value of F_B is constant, L_C is the width of the eddy current brake's magnetic field.

θ' is the angle between the target's angular velocity vector and the arm of F_B.

θ is the angle between the target's angular velocity vector and the Z axis of the target's body frame.

δ is the angle between the target's angular velocity vector and its angular momentum, calculated as the angle between H and the target's Z axis minus θ (Fig. 8).

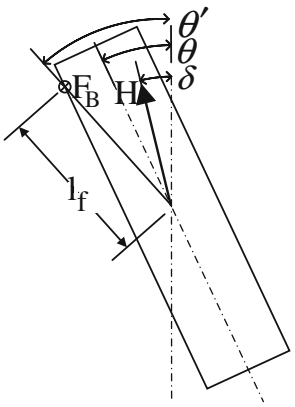

Fig. 8. Calculation of H′

The eddy-current-brake angular momentum is expressed as:

$$\begin{aligned} H_F &= F_B \cdot l_f \cdot t = F_B \cdot l_f \cdot \left(\frac{L_C}{\omega \cdot l_f \cdot \sin\theta'}\right) \\ &= \frac{F_B \cdot L_C}{\omega \cdot \sin\theta'} = \frac{K_F}{\omega} \cdot \frac{1}{\sin\theta'} \end{aligned} \tag{11}$$

Where, $K_F = F_B \cdot L_C$. Apply the law of cosines in the triangle built by H_F, H', H. The detailed process is

$$\begin{aligned} |H'|^2 &= |H|^2 + |H_F|^2 - 2 \cdot |H| \cdot |H_F| \cdot \cos\gamma \\ &= |H|^2 + |H_F|^2 - 2 \cdot |H| \cdot |H_F| \cdot \sin(\theta' + \delta) \\ &= |H|^2 + \left(\frac{K_F}{\omega} \cdot \frac{1}{\sin\theta'}\right)^2 - 2 \cdot |H| \cdot \left(\frac{K_F}{\omega} \cdot \frac{1}{\sin\theta'}\right) \cdot \sin(\theta' + \delta) \\ &= |H|^2 + \left(\frac{K_F}{\omega}\right)^2 \cdot \frac{1}{\sin^2\theta'} - 2 \cdot |H| \cdot \frac{K_F}{\omega} \cdot \frac{\sin\theta' \cdot \cos\delta + \cos\theta' \cdot \sin\delta}{\sin\theta'} \\ &= |H|^2 + \left(\frac{K_F}{\omega}\right)^2 \cdot \frac{1}{\sin^2\theta'} - 2 \cdot |H| \cdot \frac{K_F}{\omega} \cdot \frac{\cos\theta' \cdot \sin\delta}{\sin\theta'} 2 \cdot |H| \cdot \frac{K_F}{\omega} \cdot \cos\delta \end{aligned} \tag{12}$$

In the above equation, the change of the brake force's point of action will lead to the change of θ', which will affect the value of H'. Set $|H'|^2$ as the function with θ' as the independent variable:$f(\theta')$.

Calculate the function's minimum value by its first derivative:

$$f'(\theta') = -2 \cdot \left(\frac{K_F}{\omega}\right)^2 \cdot \frac{\cos\ \theta'}{sin^3\theta'} - 2 \cdot |H| \cdot \frac{K_F}{\omega} \cdot \sin\ \delta \cdot \frac{-\sin\ \theta' \cdot \sin\ \theta' - \cos\ \theta' \cdot \cos\ \theta'}{sin^2\theta'}$$
$$= 2 \cdot \left(\frac{K_F}{\omega}\right)^2 \cdot \frac{\cos\ \theta'}{sin^3\theta'} + 2 \cdot |H| \cdot \frac{K_F}{\omega} \cdot \sin\ \delta \cdot \frac{1}{sin^2\theta'} \tag{13}$$
$$= 2 \cdot \frac{K_F}{\omega} \cdot \frac{1}{sin^2\theta'} \left(|H| \cdot \sin\ \delta - \frac{K_F}{\omega} \cdot \frac{\cos\ \theta'}{\sin\ \theta'}\right)$$

$$\theta' \in \left(\theta'_{min}, \frac{\pi}{2}\right); \theta'_{min} = \theta + \tan^{-1}\left(\frac{2R}{h}\right) \tag{14}$$

Set $f'(\theta') = 0$, then:

$$\theta' = \tan^{-1}\left(\frac{K_F}{\omega|H| \cdot \sin\ \delta}\right) \tag{15}$$

It can be concluded that:

$$\begin{aligned} &f'(\theta') > 0, 0 < \theta' < \tan^{-1}\left(\frac{K_F}{\omega|H| \cdot \sin\ \delta}\right) \\ &f'(\theta') < 0, \tan^{-1}\left(\frac{K_F}{\omega|H| \cdot \sin\ \delta}\right) < \theta' < \frac{\pi}{2} \end{aligned} \tag{16}$$

Function $f(\theta')$ has its minimum value when $\theta' = \tan^{-1}\left(\frac{K_F}{\omega|H| \cdot \sin\ \delta}\right)$.

Summing up the above, the optimized de-tumbling strategy performs best when $\theta' = \tan^{-1}\left(\frac{K_F}{\omega|H| \cdot \sin\ \delta}\right)$ in the target's every spin cycle.

4 Simulation of Optimized De-Tumbling Method

4.1 Simulation

A simulation is performed to estimate the optimized method using MATLAB tools. The target's model is based on the abandoned rocket's upper stage with a launch weight of 2154 kg. The sizes are shown below, where R = 2.6 m, r = 2.5 m, h = 7.4 m Fig. 9.

Its moment of inertia around each axis are:

$$\begin{aligned} J_X &= \frac{m}{12} \cdot \left[3 \cdot \left(R^2 + r^2\right) + h^2\right] = \frac{16835\,\mathrm{m}^2}{\mathrm{kg}} \\ J_Y &= \frac{m}{12} \cdot \left[3 \cdot \left(R^2 + r^2\right) + h^2\right] = \frac{16835\,\mathrm{m}^2}{\mathrm{kg}} \\ J_Z &= \frac{m}{2} \cdot \left(R^2 + r^2\right) = \frac{14012\mathrm{m}^2}{\mathrm{kg}} \end{aligned} \tag{17}$$

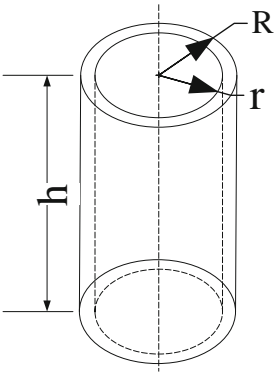

Fig. 9. Shape of target

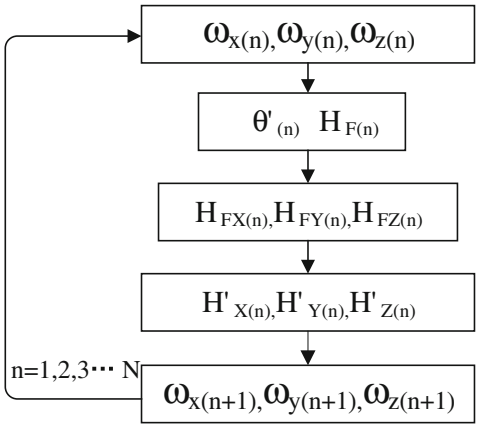

Fig. 10. Iteration cycle

Also, set the target's initial angular velocity $\omega = \frac{\pi}{18}\left(10^{\circ}\right)$ and the angle between the angular velocity and the Z axis of the target's body frame $\theta = \frac{\pi}{6}\left(30^{\circ}\right)$.

The simulation is carried out as following process, the parameters' value of every cycle is calculated by iteration Fig. 10. The angular parameters θ, θ'_{min}, δ are calculated using angular velocity data first.

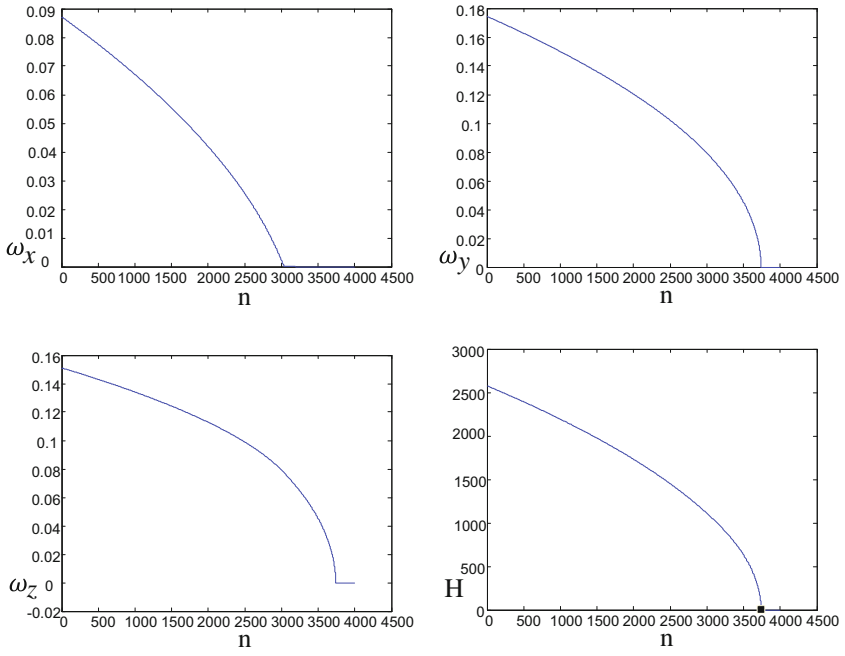

Fig. 11. Angular velocity ω_x, ω_y, ω_z, angular momentum H relative to n (iteration cycle)

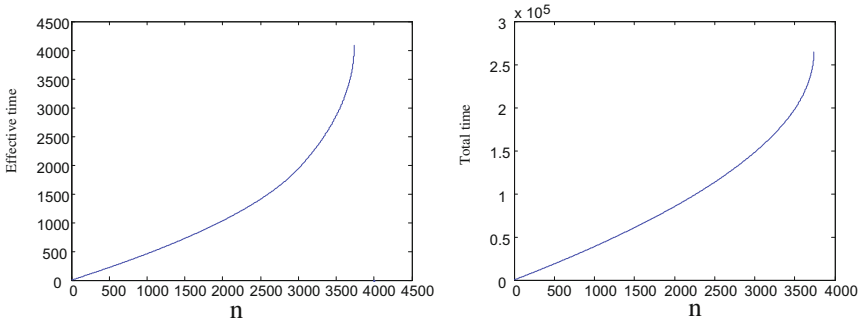

Fig. 12. Effective time of force in each cycle, Total time relative to n

Then put the angular parameters in to the Equation to calculate θ'. Then the remained angular momentum of target H' of present cycle is computed, which can be used to determine the initial angular velocity of the target's next spinning cycle.

Finish the iteration by using revolution numbers n as the iteration times. The de-tumbling process will end when H' is close to zero.

Above figures show that the target's angular velocity around each axis is gradually decreased cycle by cycle Fig. 11. But the de-tumbling rate becomes slow as the target's angular velocity slows down.

Eventually, the process stops at n = 3740 when H' is close to zero. The effective time of force in each cycle and the total time of the de-tumbling procedure can be calculated Fig. 12.

On the other hand, if the brake force's point of action is not optimized, but constantly acting at the middle part of the target Fig. 13. The simulation results as below Fig. 14:

Put the angular parameters into iteration, the total time can be computed relative to cycle time. Comparing to the total time in optimized de-tumbling, it can be concluded that the time consuming in debris removal can be spared by optimized de-tumbling strategy based on the debris' kinematic parameters of spin movement.

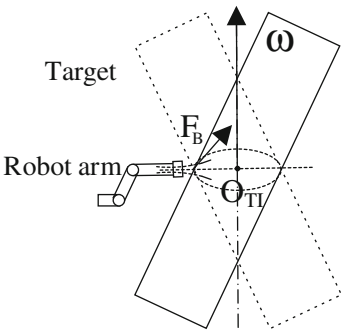

Fig. 13. Un-optimized method of de-tumbling

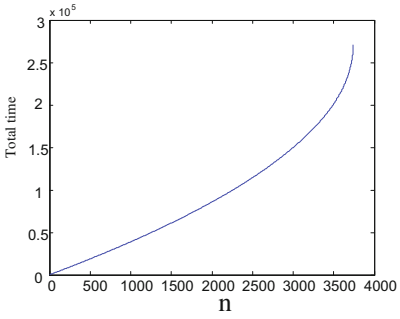

Fig. 14. Total time of un-optimized method

5 Conclusions and Future Work

In this paper, we presented our motivation for studying capturing of large tumbling target. In most cases, the space debris who loses power and control always floats freely with large residual angular momentum on-orbit. Especially when the collision occurs between debris and other objects, the residual angular momentum will increase, which will further increase the challenge of capture safety. In this paper, we propose a method of de-tumbling a large tumbling target with the eddy current brake. The eddy current brake is mounted on the hand of the manipulator to brake the tumbling target, and the residual angular momentum is reduced smaller. Thereby providing safer conditions for arm-based capture. In view of the characteristics of the motion of the large tumbling target, this paper presents an optimized method of braking, and obtains the optimized planning trajectory by simulation. Then, the validity of the above method is verified by simulation.

The effectiveness of large debris de-tumbling based on eddy current brake in hand of manipulator is verified by the study of the noncontact de-tumbling technology by the simplified model. The ground experiment based on the 6 DoF space manipulator [12] and air-bed experimental system [13] will be carried out in the future and the results should be applied to practice.

Acknowledgment. Thanks for the support of the research work by China Academy of Launch Vehicle Technology (CASC). The authors would like to acknowledge the support of the team members for their outstanding contributions to the paper.

References

1. Greaves, S., Boyle, K., Doshewnek, N.: Orbiter boom sensor system and shuttle return to flight: operations analyses. In: AIAA Guidance Navigation, and Control Conference and Exhibit, San Francisco, p. 5986 (2005)
2. Liu, J., Fan, Q., Yang, T., Li, K., Huang, Q.: A space robot manipulator system: designed for capture. Int. J. Mechatron. Autom. **5**(2/3), 125–132 (2015)
3. Shoemaker, J., Wright, M.: Orbital express space operations architecture program. Space systems technology and operations. In: Tchoryk Jr., P., Shoemaker, J. (eds.) Proceedings of SPIE, vol. 5088, pp. 1–9 (2003)
4. Gomez, N.O., Walker, S.J.I.: Eddy currents applied to de-tumbling of space debris: analysis and validation of approximate proposed methods. Acta Astronaut. **114**, 34–53 (2015)
5. Sugai, F., Abiko, S., Tsujita, T., Jiang, X., Uchiyama, M.: De-tumbling an uncontrolled satellite with contactless force by using an eddy current brake. In: Proceedings of IEEE International Conference on Intelligent Robots and Systems, Tokyo, 3–7 November 2013, pp. 783–788 (2013)
6. Reinhardt, B., Peck, M.A.: Eddy-current space tug. In: Proceedings of AIAA SPACE Conference & Exposition, Long Beach, 27–29 September 2011
7. Ambroglini, F., Battiston, R., Burger, W.J., Calvelli, V., Musenich, R., Spillantini, P., Giraudo, M., Vuolo, M.: Active magnetic shielding for manned space missions present perspectives. In: Sgobba, T., Rongier, I. (eds.) Space Safety is No Accident, pp. 151–160. Springer, Cham (2015). doi:10.1007/978-3-319-15982-9_18

8. Yoshida, K.: Engineering test satellite VII flight experiment for space robot dynamics and control: Theories on laboratory test beds ten years ago, now in orbit. Int. J. Rob. Res. **22**(5), 321–335 (2003)
9. Murray, R.M., Li, Z., Sastry, S.S.: A Mathematical Introduction to Robotic Manipulation. CRC Press, Boca Raton (1994)
10. Featherstone, R.: Robot Dynamics Algorithms. Kluwer, Norwell, MA (1987)
11. Landzettel, K., Brunner, B., Hirzinger, G., Lampariello, R., Schreiber, G., Steinmetz, B.-M.: A unified ground control and programming methodology for space robotics applications-demonstrations on ETS-VII. In: Proceedings of International Symposium on Robotics, Montreal pp. 422–427 (2000)
12. Liu, J., Fan, Q., Wang, Y., et al.: A space robot hand arm system: designed for capture. In: IEEE International Conference on Mechatronics and Automation. pp. 1247–1252 (2015)
13. Liu, J., Huang, Q., Wang, Y., Deng, T.: A method of ground verification for energy optimization in trajectory planning for six DOF space manipulator. In: Proceedings of IEEE International Conference on Fluid Power and Mechatronics, Harbin, 5–7 August 2015, pp. 791–796 (2015)